Original Article

Cytoglobin suppresses oxidative damage and compensatory proliferation via inhibiting AKT/ERK1/2/CyclinD1 axis in hepatocellular carcinoma

Siyun Yang^{1*}, Mei Cai^{1*}, Yushi Yang², Yuxin Huang², Tingjie Hou¹, Jun Zhang^{1,2}

¹Department of Pathology, Graduate School of Medicine, Guizhou Medical University, No. 9 Bei Jing Road, Guiyang 550004, Guizhou, China; ²Department of Pathology, The Affiliated Hospital of Guizhou Medical University, No. 28 Gui Yi Street, Guiyang 550004, Guizhou, China. *Equal contributors.

Received June 4, 2025; Accepted August 14, 2025; Epub September 15, 2025; Published September 30, 2025

Abstract: The chronic liver injury caused by diverse etiologies provokes abnormal compensatory proliferation and contributes to hepatocarcinogenesis. Oxidative stress (OS) is an independent etiology which induces cell injury and triggers oncogenes activation and tumor suppressor genes dysfunction. Cytoglobin (CYGB) is a member of the human hexacoordinate hemoglobin (HHB) family and functions as a dynamic antioxidant enzyme. We previously reported that CYGB decreases the intracellular ROS/RNS level and inhibits HCC proliferation and stemness under normal oxidative level. In this study, we observed that CYGB is decreased in HCC tissues, particularly in tumors with p53 mutations. Its deficiency is associated with advanced stage, elevated Ki-67 proliferation index, and predicts a worse prognosis in HCC patients. Ectopic CYGB expression attenuates malondialdehyde (MDA) level and AST/ALT release, as well reduces apoptosis and subG1 percentage and simultaneously induces G1 arrest in pre-H₂O₂-treated HCC cells. In addition, CYGB expression inhibits HCC proliferation and inactivates AKT and ERK kinases, the regulative effect can be interfered by necrostatin-1 and Z-VAD-FMK. Furthermore, UO126, the MEK1/2 inhibitor, can block the regulation of CYGB upon AKT/ERK/CyclinD1 axis, as well interfere with CYGB-induced proliferative inhibition in pre-H₂O₂ treated HCC cells, whether necrostatin-1 and Z-VAD-FMK presence or not. In conclusion, CYGB controls oxidative damage-associated molecule patterns and functions as a tumor suppressor, its restoration may provide a therapeutic target against HCC with aberrant OS response.

Keywords: Cytoglobin, oxidative damage, compensatory proliferation, AKT/ERK1/2/CyclinD1 axis, hepatocellular carcinoma

Introduction

Reactive oxygen/nitrogen species (RONS) is a dynamic substance and plays a crucial function in the processes of liver biotransformation, catabolism and signal transduction. The chronic liver injury caused by diverse etiologies breaks redox balance and results in hepatocyte abnormal oxidative stress, which contributes to hepatocellular carcinoma (HCC) genesis and development [1]. Antioxidant AKR1B10 (Aldoketo reductase 1B10) plays an important role in protecting hepatocytes from damage induced by ROS. Deficiency of AKR1B10 might accelerate hepatotoxin and inflammation-associated hepatocarcinogenesis [2]. Oxidative DNA damage induced by the dysfunction of SIRT5

(deacetylase sirtuin 5) - ACOX1 (Acyl-CoA oxidase 1) axis eventually leads to HCC development [4]. AKT activation stabilizes MDM2 structure which regulates p53 response to oxidative stress and promotes cell proliferation and carcinogen-induced HCC [5]. E-cadherin degradation mediated by OS-activated PKA promotes HCC metastasis in vitro and in vivo [6]. Damageassociated compensatory regeneration is a common pathogenesis in HCC driven by diverse etiologies. Nucleostemin (NS) protects HCC cells from replication- and drug-induced DNA damage and promotes liver regeneration via a damage repair mechanism. It supports an essential mechanism that HCC can adapt to high genomic stress and survive [7]. Oxidative stress (OS) triggers apoptotic and necrotic

mechanisms and remodels liver vasculature, which contributes to liver fibrosis, cirrhosis and liver cancers [8]. DEN (Diethylnitrosamine) provokes liver damage and oxidative stress in trem-2^{-/-} (triggering receptor expressed on myeloid cells 2) mice, whereas antioxidant diet can mitigate DEN-induced hepatocarcinogenesis in mouse model [9]. The extract of ginger inhibits cell proliferation and protects rat liver from carcinogen-induced tumorigenesis through controlling OS response and inflammatory signaling [10]. Therefore, OS functions as a dynamic regulator and involves in multi-course of HCC occurrence and progression, targeting OS provides a promising therapeutic strategy against HCC with aberrant OS response.

Cytoglobin (CYGB) is a conservative hemoglobin with iron penta- or hexa-coordinated capacity and performs the activities of antioxidant enzymes including NO dioxygenase, peroxidase and superoxide dismutase [11, 12]. Cytoglobin deletion exhibits broad changes that include a heightened inflammatory response, fibrosis, cardiovascular dysfunction and senescence, as well tumor incidences and tumor burden. It is specially deregulated in multi-malignancies, hypoxia and various stresses can regulate its expression [11, 13, 14]. Dimethylbenz(a) anthracene (DMBA)-induced pancreatic cancer incidence was 93% in wild-type mice but only 55% in CYGB-overexpressed mice. CYGB overexpression initiates G1 phase arrest, diminishes cell migration and colony formation in pancreatic cancer cells [15]. Ectopic CYGB expression suppresses breast cancer cell proliferation, migration, invasion regardless of p53 status, CYGB expression inhibits GLUT1 and HXK2 expression, it impacts glucose metabolism and inhibits xenograft tumor growth in vivo [16]. Ectopic miR-210-3p targets GPD1L and CYGB and controls glucose uptake and Warburg effect, which promotes colony formation and protects triple negative breast cancer cells from serum starvation-induced cell apoptosis [17]. CYGB promoter de-methylation induced by DNMT3B (DNA methyltransferase 3 beta) transcriptional inhibition controls bladder cancer progression and predicts a good prognosis [18]. However, CYGB enhances heme-oxygenase 1 (HO-1) and NRF2 protein expression and protects melanoma cells from RONS-induced apoptosis [19]. CYGB deficiency aggravates intracellular ROS accumulation and lipid peroxidation and sensitizes melanoma cells to ferroptosis, its knockdown activates inflammasome and promotes pyroptosis [20]. Collectively, CYGB restoration can inhibit tumor growth and progression *in vitro* and *in vivo*, it can also protect tumor cells from stress-induced cell damage, thus the anti-tumor effects and underlying mechanisms of CYGB need to be further explored.

We reported that CYGB is significantly decreased in human HCC tissue, ectopic CYGB expression inhibits HCC proliferation and stemness at a ROS/RNS-dependent manner [21]. In this study, we investigated the association of CYGB differential expression with clinicopathologic characteristics, as well the effects and mechanisms of CYGB upon OS-induced cell injury and proliferation. The results showed that CYGB deficiency confers HCC aggressive biological behaviors including large tumor mass, advanced stage, poor differentiation and predicts a worse prognosis. The mechanistic studies found that CYGB can maintain homoeostasis and controls oxidative damage-associated AKT/ERK activation and subsequently compensatory proliferation.

Materials and methods

Human HCC samples and immunohistochemistry (IHC) analysis

123 cases of human HCC samples were collected from surgically resected tissues in the Affiliated Hospital of Guizhou Medical University during 2018 to 2021. The project is approved by the ethics committee of this institute (Approved number: 2024174). The related clinicopathological information was simultaneously collected. The CYGB, TP53 and Ki-67 expression was respectively evaluated in these HCC tissues using the primary antibodies against CYGB (SC365246, Santa Cruz Biotechnology, Inc., Shanghai, China), TP53 (ZM-0408, ZSGB-BIO Inc., Beijing, China) and Ki-67 (GT2094, GeneTech Company, Shanghai, China) by IHC staining. The brown particles observed in cytoplasm are interpreted as CYGB positive expression. IHC analysis of CYGB expression was performed as previously described with some modification in ref. [22]. The total score is ranged from 0 to 12. "≤ 6" is interpreted as low expression and "> 7" is interpreted as high expression. The brown particles observed in nuclei are interpreted as Ki-67 or p53 expression in their corresponding staining slides. More than 60% diffusely positive expression or loss expression of p53 is interpreted as p53 mutant expression. Intersperse positive cells are considered as p53 wild-type expression [23].

Cell lines, lentivirus and transfection

The human hepatocellular carcinoma cell lines HepG2, Hep3B and Huh7 were purchased from the National Collection of Authenticated Cell Cultures (Shanghai, China). These cell lines were cultured in ATCC recommended medium supplemented with 10% (v/v) fetal bovine serum (FBS) and 100 µg/ml penicillin-streptomycin at 37°C in a 95% humidity incubator containing 5% carbon dioxide. The CYGB-expressing lentivirus or its control was purchased from Genechem (Shanghai, China). The full-length sequence of CYGB was inserted into LVCON335 to construct a CYGB-expressing lentivirus, and LVCON335 (Ubi-MCS-3FLAG-CBh-gcGFP-IRESpuromycin) was used as the control. The lentivirus transfection was performed according to the manufacturer's instructions. The transfected cells were selected using puromycin. Transfection efficiency was identified by gPCR and western blotting.

Chemicals and reagents

Ferrostatin-1 (S7243), necrostatin-1 (S8037) and Z-VAD-FMK (S7023) are respectively the inhibitors of ferroptosis, receptor-interacting protein kinase 1 (RIPK1) and caspases and were purchased from Selleck (Shanghai, China). U0126 is the inhibitor of was bought from Cell signaling technology (Danver, USA). The primary antibodies against p53, cyclinD1, phospho-JNK (Thr183/Tyr185), JNK, phospho-AKT (Ser473), AKT, phospho-ERK1/2 (Thr202/Tyr204) and ERK1/2 and were bought from Cell Signaling Technology (Danver, USA). GAPDH antibody was bought from Genetex (USA).

Real-time quantitative PCR

Total RNA was extracted using RNA-QUICK Purification Kit (ES Science, Shanghai, China), subsequently it was reversely transcribed to cDNA using Fast All-in-One RT KIT (ES Science, Shanghai. China), according to the manufacturer's instruction. 2 ug cDNAs was quantitatively

analyzed using Super SYBR Green qPCR Master Mix (ES Science, Shanghai, China) in real-time PCR system (CFX Connect Real-Time System, Bio-RAD Inc.). Primer sequences of target genes are shown as followed:

Targeted cDNA	Primer sequence (5'-3')	Product length
CYGB	Forward 5'-CACAAGGTGGAACCGGTGTA-3' Reverse 5'-CCCGAAGAGGGCAGTGTGG-3'	218 bp
GAPDH	Forward 5'-AAGAAGGTGGTGAAGCAGG-3' Reverse 5'-GTCAAAGGTGGAGGAGTGG-3'	114 bp

Cell viability assay and EdU-incorporation assay

2000-3000 HCC cells were seeded in 96-well dark plate overnight to permit appropriate attachment, and cell viability was assessed within 5 days using MTT Cell Proliferation and Toxicity Kit (Solarbio, Beijing, China), according to the manufacturer's instructions. 490 nm absorbance of the solution was measured using an EnSpire Multilabel Plate Reader (Perkin Elmer, USA).

10000 HCC cells were seeded in 24-well dark plate with the corresponding treatment. Cell proliferation was assessed using Cell-Light EdU Apollo In Vitro Kit (Ribobio, Guangzhou, China) according to the manufacturer's instructions. Fluorescent images were taken randomly from at least six different fields in each well with a conventional inverted fluorescent microscope (Leica DM4B, Leica, Germany).

Cell cycle profile and apoptosis detection

Cells were cultured in serum-free medium for 24 h to induce G1 phase synchronization and were collected at the indicated time points with the corresponding treatment. Then the cells were stained with propidium iodide (Sigma) at a final concentration of 0.1 mg/ml for 15 minutes and DNA content was measured using flow cytometer (FACSCalibur™, Becton, Dickinson and Company, USA). Cell cycle curve was fitted using modFit LT 5.0 software.

HCC cells were treated using $1 \, \text{mM H}_2 O_2$ for $15 \, \text{min}$ and subsequently were cultured in the fresh medium for $12 \, \text{h}$ to induce apoptosis. The apoptotic cells were labeled using Annexin V-APC/7-AAD apoptosis kit (MUITI Sciences, Hangzhou, China), then the apoptotic percent-

age was calculated and analyzed using flow cytometer (FACSCalibur TM , Becton, Dickinson and Company, USA).

Extracellular alanine and aspartate aminotransferase (ALT and AST) assay and Intracellular malondialdehyde (MDA) assay

10000 HCC cells were seeded 6-well plate with or without $\operatorname{pre-H_2O_2}$ treatment. These cultured medium were collected at the indicated time points, then ALT or AST content in the medium were respectively detected to assess HCC cell injury as previously discribed [24] using alanine aminotransferase assay kit or aspartate aminotransferase assay kit (Nanjing Jiancheng Bioengineering institute, Nanjing, China), according to the manufacturer's instructions. 510 nm absorbance of the solution was measured using an EnSpire Multilabel Plate Reader (Perkin Elmer, USA).

10000 HCC cells were seeded 6-well plate with or without pre- $\rm H_2O_2$ treatment and intracellular MDA content were assessed using cellular MDA assay kit (Nanjing Jiancheng Bioengineering institute, Nanjing, China), according to the manufacturer's instructions. 530 nm absorbance of the solution was measured using an EnSpire Multilabel Plate Reader (Perkin Elmer, USA).

Public data collection and survival assessment

GEPIA (Gene Expression Profiling Interactive Analysis) (cancer-pku.cn) is a newly developed interactive web server for analyzing the RNA sequencing expression data of 9,736 tumors and 8,587 normal samples from the TCGA and the GTEx projects [25]. It provides the prognostic analysis of liver hepatocellular carcinoma (LIHC) with CYGB expression from TCGA database.

Protein simulative modeling and molecular docking analysis

The protein primary and spatial structure was constructed and extracted from RCSB Protein Data Bank (RCSB PDB) (https://rcsb.org/), then the protein structure information was provided to HDOCK server (http://hdock.phys. hust.edu.cn/), which automatically analyzes molecular docking modeling through a hybrid algorithm of template-based and template-free

docking and predicts their affinity and docking sites between the submitted proteins. The docking score reflects the affinitive capacity [26].

Western blotting

Cells were lysed using RIPA buffer containing 1% phenylmethylflavinyl fluoride (PMSF) (Beyotime, Nantong, China) and total protein was collected and quantified using Bio-Rad Bradford reagents (Bio-Rad Laboratories, Hercules, CA). 10-20 µg of equal amount proteins were separated in SDS-PAGE gels using the XCell system (Invitrogen). The proteins were transferred into PVDF membranes using a transfer apparatus (Bio-Rad). The blots were incubated with the primary antibodies at 4°C temperature overnight, the HRP-conjugated secondary antibodies were used and the bands were visualized using ChemiDocTMMP imaging System (BIO-RAD). The average optical density of the band was measured using ImageJ software.

Statistical analysis

Comparison of categorical variables including two or three sample rates was evaluated using Chi-square tests. A two-way ANOVA analysis was used to determine significant differences between groups that had been split on two independent variables. Post-hoc testing for the ANOVA was performed using the Tukey method. The correlation of CYGB expression with Ki67 index in human HCC samples was analyzed using pearson's correlation analysis. Cell experiments were independently repeated no less than three times. Data are presented as mean \pm standard error. *P*-value less than 0.05 were considered statistical significance and all data were analyzed using GraphPad 9.0 software.

Results

CYGB deficiency is associated with advanced stage and poor differentiation, as well predicts a worse prognosis

We detected CYGB expression in 123 human hepatocellular carcinoma tissues and analyzed its association with clinicopathological characteristics. The results show that CYGB is decreased in HCC tissues (21.1%, 26/123), compared with these adjacent non-tumor tissues (ANT) (78.8%, 89/113) (Figure 1A and

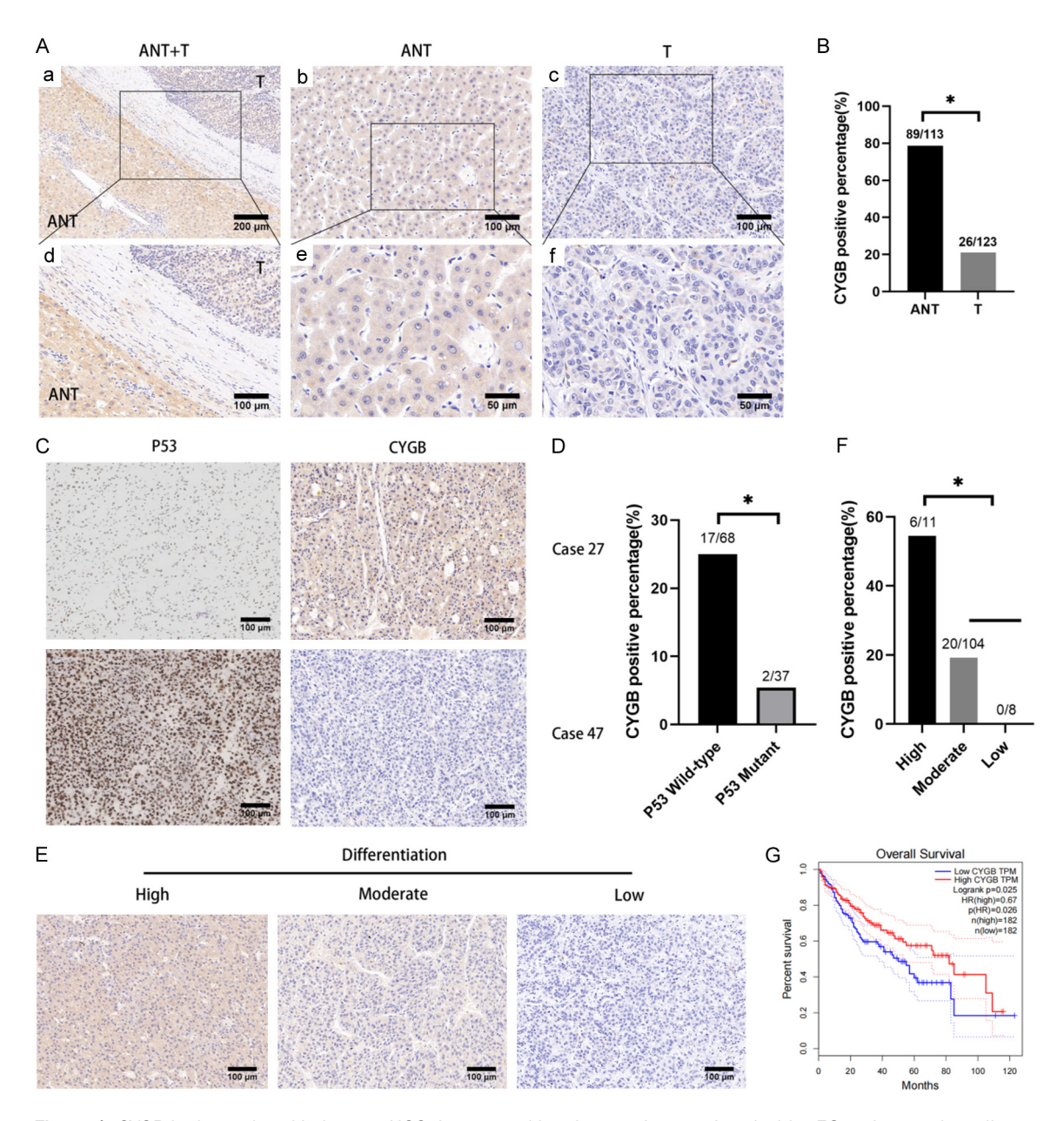


Figure 1. CYGB is deregulated in human HCC tissues and its absence is associated with p53 variant and predicts a poor prognosis. (A and B) The expression of CYGB in 123 cases of human HCC tissues and these adjacent non-tumor tissues was assessed. "T" and "ANT" respectively represents HCC tumor tissues and these adjacent non-tumor tissues. (A) These representative images of CYGB expression in HCC tissues are shown at the indicated magnification (a with 100× magnification; b, c and d with 200× magnification; e and f with 400× magnification). (B) The CYGB positive percentage were calculated and statistically analyzed (Chi-square test or fisher's exact test, "*" represents P < 0.05). (C and D) The correlation of CYGB expression with p53 status was detected and analyzed in this cohort. (C) The representative images of CYGB and p53 expression are shown in the identical HCC sample with 200× magnification. (D) The positive percentage of CYGB were calculated and statistically analyzed (Chi-square test or fisher's exact test, "*" represents P < 0.05). (E and F) The expression of CYGB in HCC tissues with different differentiation was evaluated. (E) These representative images of CYGB expression in HCC tissues are shown with 200× magnification. (F) The CYGB positive percentage were calculated and statistically analyzed. HCC samples with the low and moderate differentiation are integrated as a high-grade group for statistical analysis. (Chi-square test or fisher's exact test, "*" represents P < 0.05). (G) The overall survival of HCC patients with CYGB differential expression was extracted from TCGA database and was analyzed using GEPIA web server. The overall survival curve is shown.

1B). TP53 status is also evaluated and the result show that CYGB expression is increased

in HCC tissues harboring with wild-type p53 (17/68, 25.0%) (**Figure 1C** and **1D**). Meanwhile,

Table 1. The association of CYGB expression with clinicopathological characteristics in HCC

Sex	Daramatara	CYGB protein		. X ²	n volus		
male female 76 (76.0%) 24 (24.0%) 2.627 0.105 Age ≥ 60 32 (72.7%) 12 (27.3%) 1.547 0.214 < 60	Parameters	Low (≤ 6)	High (> 7)	Χ-	p value		
female 21 (91.3%) 2 (8.7%) Age ≥ 60 32 (72.7%) 12 (27.3%) 1.547 0.214 < 60	Sex						
Age ≥ 60 32 (72.7%) 12 (27.3%) 1.547 0.214 < 60	male	76 (76.0%)	24 (24.0%)	2.627	0.105		
≥ 60 32 (72.7%) 12 (27.3%) 1.547 0.214 < 60	female	21 (91.3%)	2 (8.7%)				
< 60 65 (82.3%) 14 (17.7) $<$ $<$ $<$ $<$ $<$ $<$ $<$ $<$ $<$ $<$ $<$ $<$ $<$ $<$ $<$ $<$ $<$ $<$ $<$ $<$ $<$ $<$ $<$ $<$ $<$ $<$ $<$ $<$ $<$ $<$ $<$ $<$ $<$ $<$ $<$ $<$ $<$ $<$ $<$ $<$ $<$ $<$ $<$ $<$ $<$ $<$ $<$ $<$ $<$ $<$ $<$ $<$ $<$ $<$ $<$ $<$ $<$ $<$ $<$ $<$ $<$ $<$ $<$ $<$ $<$ $<$ $<$ $<$ $<$ $<$ $<$ $<$ $<$ $<$ $<$ $<$ $<$ $<$ $<$ $<$ $<$ $<$ $<$ $<$ $<$ $<$ $<$ $<$ $<$ $<$ $<$ $<$ $<$ $<$ $<$ $<$ $<$ $<$ $<$ $<$ $<$ $<$	Age						
HBsAg infection Yes 74 (79.6%) 19 (20.4%) 0.115 0.735 No 23 (76.7%) 7 (23.3%) Serum AFP < 400 ng/ml	≥ 60	32 (72.7%)	12 (27.3%)	1.547	0.214		
Yes 74 (79.6%) 19 (20.4%) 0.115 0.735 No 23 (76.7%) 7 (23.3%) \cdot \cdot Serum AFP \cdot \cdot \cdot \cdot \cdot \cdot 400 ng/ml 67 (78.8%) 18 (21.2%) 0.000 0.988 \cdot 400 ng/ml 30 (78.9%) 8 (21.1%) \cdot \cdot AST/ALT \cdot	< 60	65 (82.3%)	14 (17.7)				
No 23 (76.7%) 7 (23.3%) Image: Control of the con	HBsAg infection						
Serum AFP $<$ 400 ng/ml 67 (78.8%) 18 (21.2%) 0.000 0.988 ≥ 400 ng/ml 30 (78.9%) 8 (21.1%) $<$ $<$ AST/ALT $<$ $<$ $<$ $<$ $<$ < 1 25 (69.4%) 11 (30.6%) 5.739 0.017 ≥ 1 61 (88.4%) 8 (11.6%) $<$ $<$ Tumor diameter $<$ $<$ $<$ $<$ $<$ ≤ 2 cm 19 (61.3%) 12 (38.7%) $<$ $<$ $<$ $<$ > 2 cm and ≤ 5 cm 43 (86.0%) $<$ $<$ $<$ $<$ $<$ $<$ $<$ $<$ $<$ $<$ $<$ $<$ $<$ $<$ $<$ $<$ $<$ $<$ $<$ $<$ $<$ $<$ $<$ $<$ $<$ $<$ $<$ $<$ $<$ $<$ $<$ $<$ $<$ $<$ $<$ $<$ $<$ $<$ $<$ $<$ $<$ $<$ $<$ $<$ $<$ $<$ $<$ $<$ $<$ $<$	Yes	74 (79.6%)	19 (20.4%)	0.115	0.735		
	No	23 (76.7%)	7 (23.3%)				
≥ 400 ng/ml 30 (78.9%) 8 (21.1%) AST/ALT 25 (69.4%) 11 (30.6%) 5.739 0.017 ≥ 1 61 (88.4%) 8 (11.6%) ** ** Tumor diameter 19 (61.3%) 12 (38.7%) 7.774 0.021 > 2 cm and ≤ 5 cm 43 (86.0%) 7 (14.0%) ** ** > 5 cm 35 (83.3%) 7 (16.7%) ** ** Differentiation ** 43 (86.0%) 7 (16.7%) ** ** Low-grade 5 (45.5%) 6 (54.5%) 8.088 0.004 High-grade* 92 (81.2%) 20 (17.9%) ** ** Clinical stage 1+II 77 (75.5%) 25 (24.5%) 4.074 0.044 III+IV 20 (95.2%) 1 (4.8%) ** ** Peritoneal violation Yes 19 (86.4%) 3 (13.6%) 0.904 0.342 No 78 (77.2%) 23 (22.8%) ** ** MVI** Yes 31 (88.6%) 4 (11.4%) 2.767 0.096 No 66 (75.0%) 22 (25.0%) ** <td< td=""><td>Serum AFP</td><td></td><td></td><td></td><td></td></td<>	Serum AFP						
AST/ALT < 1	< 400 ng/ml	67 (78.8%)	18 (21.2%)	0.000	0.988		
	≥ 400 ng/mI	30 (78.9%)	8 (21.1%)				
	AST/ALT						
Tumor diameter ≤ 2 cm 19 (61.3%) 12 (38.7%) 7.774 0.021 > 2 cm and ≤ 5 cm 43 (86.0%) 7 (14.0%) > 5 cm 35 (83.3%) 7 (16.7%) Differentiation Low-grade 5 (45.5%) 6 (54.5%) 8.088 0.004 High-grade* 92 (81.2%) 20 (17.9%) Clinical stage I+II 77 (75.5%) 25 (24.5%) 4.074 0.044 III+IV 20 (95.2%) 1 (4.8%) Peritoneal violation Yes 19 (86.4%) 3 (13.6%) 0.904 0.342 No 78 (77.2%) 23 (22.8%) MVI** Yes 31 (88.6%) 4 (11.4%) 2.767 0.096 No 66 (75.0%) 22 (25.0%) Cirrhosis 48 (78.7%) 13 (21.3%) 0.002 0.963	< 1	25 (69.4%)	11 (30.6%)	5.739	0.017		
≤ 2 cm 19 (61.3%) 12 (38.7%) 7.774 0.021 > 2 cm and ≤ 5 cm 43 (86.0%) 7 (14.0%)	≥ 1	61 (88.4%)	8 (11.6%)				
> 2 cm and ≤ 5 cm 43 (86.0%) 7 (14.0%) > 5 cm 35 (83.3%) 7 (16.7%) Differentiation Low-grade 5 (45.5%) 6 (54.5%) 8.088 0.004 High-grade* 92 (81.2%) 20 (17.9%) Clinical stage I+II 77 (75.5%) 25 (24.5%) 4.074 0.044 III+IV 20 (95.2%) 1 (4.8%) Peritoneal violation Yes 19 (86.4%) 3 (13.6%) 0.904 0.342 No 78 (77.2%) 23 (22.8%) MVI** Yes 31 (88.6%) 4 (11.4%) 2.767 0.096 No 66 (75.0%) 22 (25.0%) Cirrhosis 48 (78.7%) 13 (21.3%) 0.002 0.963	Tumor diameter						
> 5 cm 35 (83.3%) 7 (16.7%) Differentiation 5 (45.5%) 6 (54.5%) 8.088 0.004 High-grade* 92 (81.2%) 20 (17.9%) Clinical stage 1+II 77 (75.5%) 25 (24.5%) 4.074 0.044 III+IV 20 (95.2%) 1 (4.8%) Peritoneal violation Yes 19 (86.4%) 3 (13.6%) 0.904 0.342 No 78 (77.2%) 23 (22.8%) MVI** Yes 31 (88.6%) 4 (11.4%) 2.767 0.096 No 66 (75.0%) 22 (25.0%) Cirrhosis 48 (78.7%) 13 (21.3%) 0.002 0.963	≤ 2 cm	19 (61.3%)	12 (38.7%)	7.774	0.021		
Differentiation Low-grade 5 (45.5%) 6 (54.5%) 8.088 0.004 High-grade* 92 (81.2%) 20 (17.9%) Clinical stage 4.074 0.044 III+IV 20 (95.2%) 1 (4.8%) Peritoneal violation 0.904 0.342 No 78 (77.2%) 23 (22.8%) MVI** Yes 31 (88.6%) 4 (11.4%) 2.767 0.096 No 66 (75.0%) 22 (25.0%) Cirrhosis 48 (78.7%) 13 (21.3%) 0.002 0.963	> 2 cm and \leq 5 cm	43 (86.0%)	7 (14.0%)				
Low-grade 5 (45.5%) 6 (54.5%) 8.088 0.004 High-grade* 92 (81.2%) 20 (17.9%) Clinical stage 4.074 0.044 III+IV 20 (95.2%) 1 (4.8%) Peritoneal violation 0.904 0.342 No 78 (77.2%) 23 (22.8%) MVI** 2.767 0.096 No 66 (75.0%) 22 (25.0%) Cirrhosis 48 (78.7%) 13 (21.3%) 0.002 0.963	> 5 cm	35 (83.3%)	7 (16.7%)				
High-grade* 92 (81.2%) 20 (17.9%) University Clinical stage 1+II 77 (75.5%) 25 (24.5%) 4.074 0.044 III+IV 20 (95.2%) 1 (4.8%)	Differentiation						
Clinical stage I+II 77 (75.5%) 25 (24.5%) 4.074 0.044 III+IV 20 (95.2%) 1 (4.8%) Peritoneal violation Yes 19 (86.4%) 3 (13.6%) 0.904 0.342 No 78 (77.2%) 23 (22.8%) MVI** Yes 31 (88.6%) 4 (11.4%) 2.767 0.096 No 66 (75.0%) 22 (25.0%) Cirrhosis 48 (78.7%) 13 (21.3%) 0.002 0.963	Low-grade	5 (45.5%)	6 (54.5%)	8.088	0.004		
I+II 77 (75.5%) 25 (24.5%) 4.074 0.044 III+IV 20 (95.2%) 1 (4.8%) Peritoneal violation 0.904 0.342 No 78 (77.2%) 23 (22.8%) MVI** 2.767 0.096 No 66 (75.0%) 22 (25.0%) Cirrhosis 48 (78.7%) 13 (21.3%) 0.002 0.963	High-grade*	92 (81.2%)	20 (17.9%)				
III+IV 20 (95.2%) 1 (4.8%) Peritoneal violation 19 (86.4%) 3 (13.6%) 0.904 0.342 No 78 (77.2%) 23 (22.8%) 5 (22.8%) 5 (22.8%) 5 (22.8%) 6 (22.8%) 6 (22.8%) 6 (22.8%) 6 (22.8%) 6 (22.8%) 6 (22.8%) 6 (22.8%) 6 (22.8%) 6 (22.8%) 6 (22.8%) 6 (22.8%) 6 (22.8%) 7 (22.	Clinical stage						
Peritoneal violation Yes 19 (86.4%) 3 (13.6%) 0.904 0.342 No 78 (77.2%) 23 (22.8%) 5 (22.8%) 5 (22.8%) 5 (22.8%) 6 (22.8%) 7 (22.8%) 7 (22.8%) 7 (22.8%) 7 (22.8%) 7 (22.8%) 7 (22.8%) 7 (22.8%) 7 (22.8%) 7 (22.8%) 7 (22.8%) 7 (22.8%) 7 (22.8%) 7 (22.8%) 7 (22.8%) 7 (22.8%) <	I+II	77 (75.5%)	25 (24.5%)	4.074	0.044		
Yes 19 (86.4%) 3 (13.6%) 0.904 0.342 No 78 (77.2%) 23 (22.8%) *** *** MVI** 31 (88.6%) 4 (11.4%) 2.767 0.096 No 66 (75.0%) 22 (25.0%) *** *** Cirrhosis 48 (78.7%) 13 (21.3%) 0.002 0.963	III+IV	20 (95.2%)	1 (4.8%)				
No 78 (77.2%) 23 (22.8%) MVI** 23 (22.8%) Yes 31 (88.6%) 4 (11.4%) 2.767 0.096 No 66 (75.0%) 22 (25.0%) Ves 48 (78.7%) 13 (21.3%) 0.002 0.963	Peritoneal violation						
MVI** Yes 31 (88.6%) 4 (11.4%) 2.767 0.096 No 66 (75.0%) 22 (25.0%) Use Use 48 (78.7%) 13 (21.3%) 0.002 0.963	Yes	19 (86.4%)	3 (13.6%)	0.904	0.342		
Yes 31 (88.6%) 4 (11.4%) 2.767 0.096 No 66 (75.0%) 22 (25.0%)	No	78 (77.2%)	23 (22.8%)				
No 66 (75.0%) 22 (25.0%) Cirrhosis Yes 48 (78.7%) 13 (21.3%) 0.002 0.963	MVI**						
Cirrhosis Yes 48 (78.7%) 13 (21.3%) 0.002 0.963	Yes	31 (88.6%)	4 (11.4%)	2.767	0.096		
Yes 48 (78.7%) 13 (21.3%) 0.002 0.963	No	66 (75.0%)	22 (25.0%)				
	Cirrhosis						
No 49 (79.0%) 13 (21.0%)	Yes	48 (78.7%)	13 (21.3%)	0.002	0.963		

[&]quot;High-grade*" includes lowly and moderately differentiated HCC samples; "MVI**" represents microvessel invasion.

it is decreased in p53-mutant HCC tissues (2/37, 5.4%) (Figure 1C and 1D). The low expression of CYGB is associated with large tumor mass, advanced clinical stage and poor differentiation (Table 1; Figure 1E and 1F). In addition, we don't observe the significant association of CYGB differential expression with gender, age, HBV infection, serum AFP level and tumor capsule and microvessel invasion in

this cohort. AST and ALT is the tissue-specific enzyme, which can be released from the injured hepatocytes. The ratio of serum AST with ALT is a sensitive indicator to assess liver injury. Interestingly, the low expression of CYGB is associated with low serum AST/ALT level (Table 1). The bio-information analysis revealed that the low CYGB expression predicts a worse overall survival in HCC patients, compared with these patients with CYGB high-expression (Figure 1G).

CYGB overexpression inhibits HCC cell growth and prevents pre-treated $\rm H_2O_2$ -induced cell injury

We constructed the stably CYGBexpressed HCC cells and confirmed its efficacy, the result show that CYGB is successfully overexpressed in HCC cells at RNA level (Figure 2A) and protein level (Figure 2B). We evaluated the effect of CYGB upon HCC cell growth, cell viability assay show that CYGB overexpression significantly inhibits HepG2 and Huh7 cell growth within 5 days (Figure 2C). AST and ALT of these tissue-specific enzymes is released from the injured hepatocyte, AST/ALT content in the medium was detected to indirectly reflect the level of HCC cell injury as previously discribed [24]. In this study, 1 mM hydrogen peroxide (H_oO_o) is used to treat HCC cells for 15 minute, subsequently these HCC cells are preserved in the fresh medium for the indicated time period to induce a sustaining oxidative injury as previously described with some modification [27]. The result showed that oxidative injury can maintain after 1 mM H₂O₂ pre-treatment for 0 h, 12 h, 16 h and 24 h (Figure 2D and 2E) using AST/ALT release experi-

ment. Furthermore, CYGB expression can significantly reduce AST/ALT release from HCC cells after 1 mM $\rm H_2O_2$ pre-treatment for 12 h, 16 h and 24 h (**Figure 2D** and **2E**). In addition, HepG2 cells were treated with or without 2 mol/L $\rm H_2O_2$ for 15 min and the medium were immediately collected to assess AST/ALT content (**Figure 2F** and **2G**), the result showed that-CYGB overexpression hasn't an immediate pro-

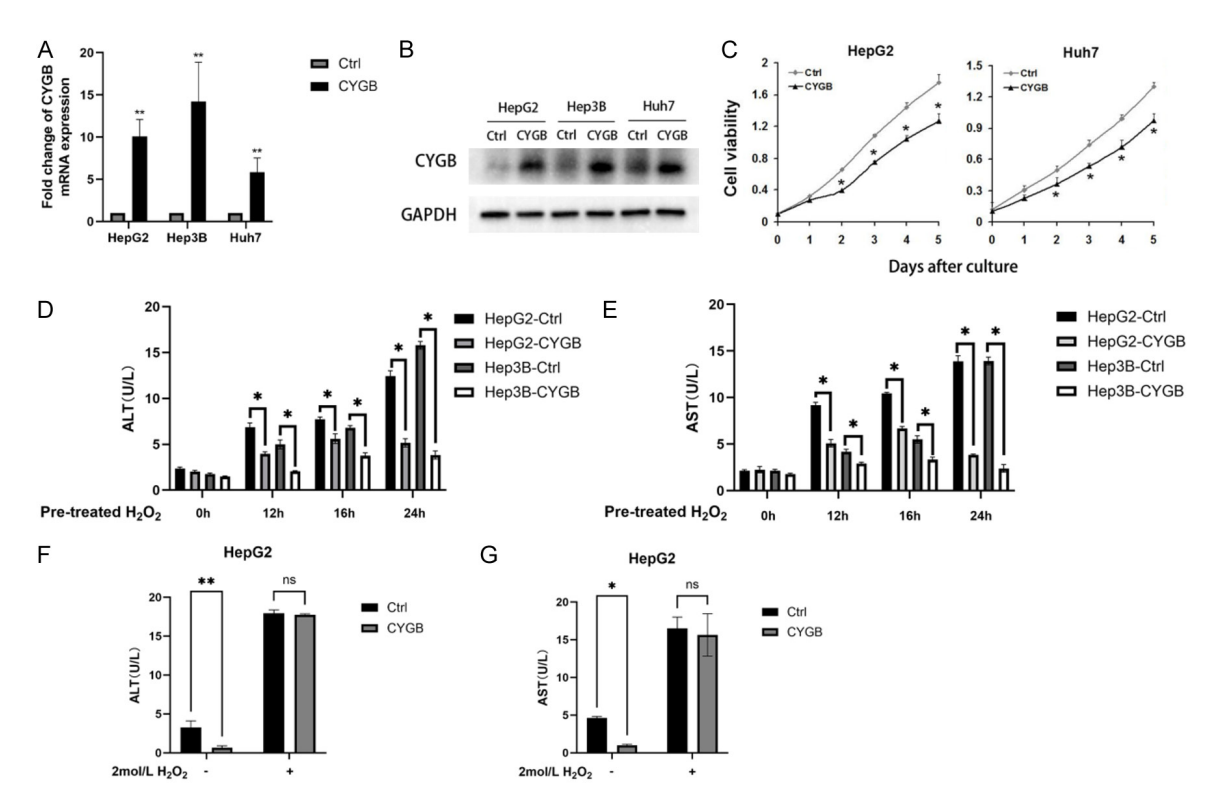


Figure 2. CYGB induces HCC cell growth inhibition and protects HCC cells from pre- $\mathrm{H_2O_2}$ -induced injury. (A and B) The efficiency of ectopic CYGB expression in RNA level (A) and protein level (B) were assessed. (C) MTT assay evaluated the viability of HepG2 and Huh7 cells within 5 days. Data are shown as Mean \pm SEM (Two-way ANOVA, "*" represents P < 0.05). (D and E) HepG2 and Hep3B cells were cultured in the medium containing 1mM $\mathrm{H_2O_2}$ for 15 min, and then the medium were replaced with the fresh medium which were collected and were are subjected to soluble ALT (D) and AST (E) content detection at the indicated time-points. Data are shown as Mean \pm SEM (Two-way ANOVA, "*" represents P < 0.05). (F and G) HepG2 cells were cultured in the medium containing 2 mol/L $\mathrm{H_2O_2}$ for 15 min, and then the medium were collected and were subjected to soluble ALT (F) and AST (G) content detection immediately. Data are shown as Mean \pm SEM (Two-way ANOVA, "*" represents P < 0.05, "**" represents P < 0.01).

tection for HCC cells treated with 2 mol/L $\rm H_2O_2$ for 15 min (**Figure 2F** and **2G**). The data suggested that CYGB has an intriguingly dual effects, it doesn't only inhibit HCC cell growth but also protects HCC cells from pre- $\rm H_2O_2$ induced oxidative injury in a delayed response manner.

CYGB prevents OS-induced apoptosis and DNA damage, as well controls cell cycle progression in pre-H₂O₂ treated HCC cells

We reported that CYGB can reduce intracellular ROS and RNS level in HCC cells [21]. Malondialdehyde (MDA) is a metabolic product in OS-dependent lipid peroxidation injury and it is an important indicator of intracellular OS level. In this study, we found that CYGB expression can significantly decrease MDA level in HepG2 cells with or without pre- ${\rm H_2O_2}$ treatment. The regulation of CYGB on MDA content can be

observed in Hep3B and Huh7 cells under pre-H₂O₂ treatment condition (Figure 3A). Flow cytometry analysis show that CYGB overexpression reduces pre-H₂O₂-induced apoptosis in HCC cells. The apoptotic inhibitory percentage is approximately for 16% in HepG2 cells and 15% in Hep3B cells with pre-H₂O₂ treatment for 12 h (Figure 3B and 3C). Cell cycle profiles show that CYGB decreases pre-H2O2-induced cell death and simultaneously induces G1 phase arrest. The result show that CYGB can respectively decrease SubG1 percentage for 8% and 11% in pre-H₂O₂ treated HepG2 cells for 12 h and 16 h (Figure 3D and 3E), simultaneously induce G1 phase arrest approximately 17% in pre-H₂O₂ treated HepG2 cells for 12 h and 16 h (Figure 3D and 3F). Suggesting that CYGB functions as a dynamic antioxidant, it protects HCC cells from oxidative injury and simultaneously induces G1 phase arrest.

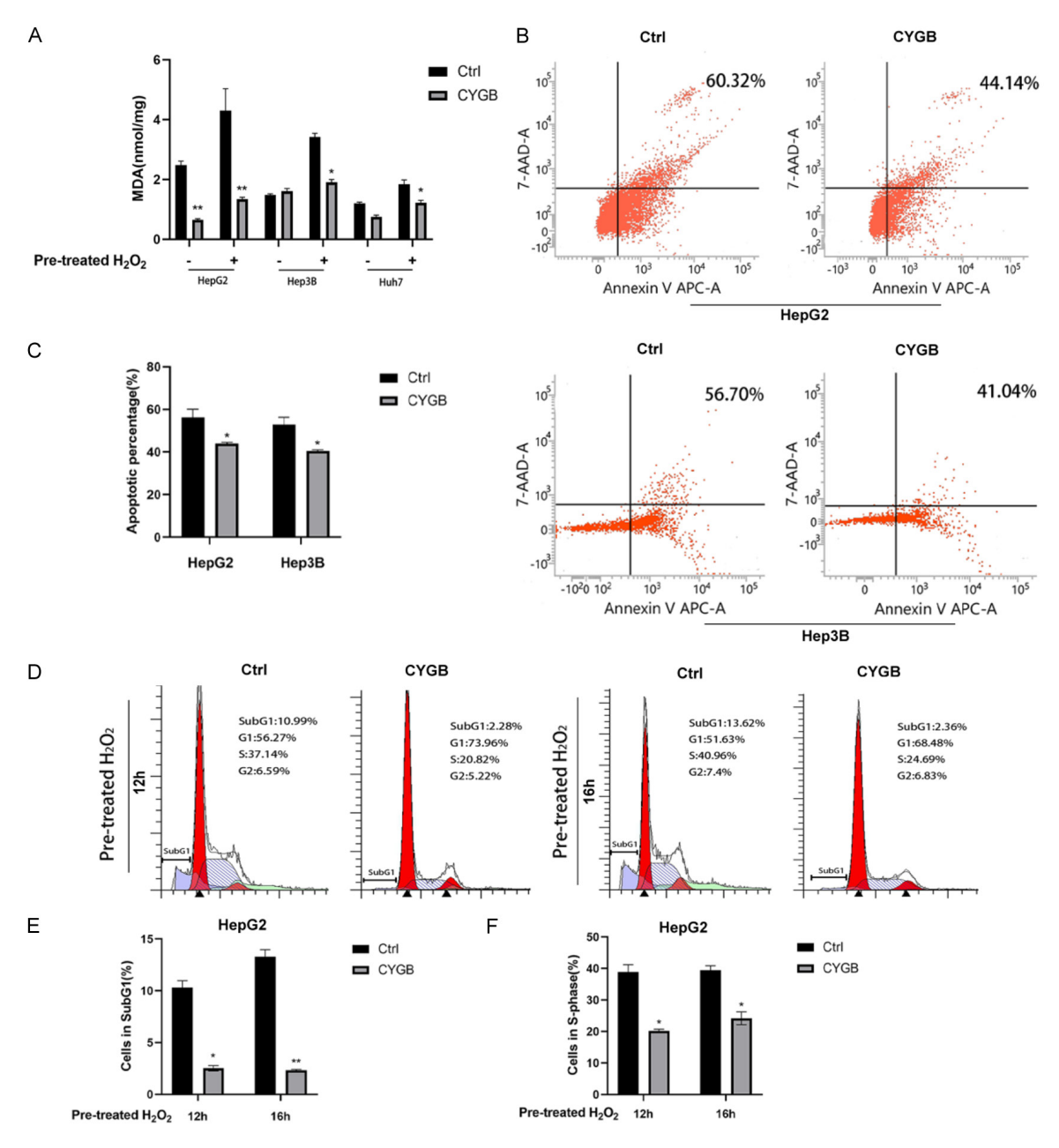


Figure 3. CYGB inhibits OS-induced cell death and induces G1 phase arrest in pre- ${\rm H_2O_2}$ treated HCC cells. A. The MDA contents were measured in HCC cells with pre- ${\rm H_2O_2}$ treated for 24 h. Data are shown as Mean \pm SEM (Two-way ANOVA, "*" represents P < 0.05). B and C. Flow cytometry assessed the apoptosis of pre- ${\rm H_2O_2}$ treated HCC cells at 12 h. B. The representative images of apoptotic analysis are shown. C. The apoptotic percentage is calculated and statistically analyzed. Data are shown as Mean \pm SEM (Two-way ANOVA, "*" represents P < 0.05). D-F. HepG2 cells were treated with pre- ${\rm H_2O_2}$ at the indicated time-point, and cells were collected and subjected to flow cytometry analysis. D. The representative cell cycle profiles are showed. E. The SubG1 percentage is statistically analyzed. Data are shown as Mean \pm SEM (Two-way ANOVA, "*" represents P < 0.05, "**" represents P < 0.01). F. These cells in S phase are calculated and statistically analyzed. Data are shown as Mean \pm SEM (Two-way ANOVA, "*" represents P < 0.05).

The proliferative inhibition of CYGB is blocked by necrostatin-1 or Z-VAD-FMK in pre-H $_2$ O $_2$ treated HCC cells

We reported that CYGB and neuroglobin (Ngb), another member of human hexacoordinate

hemoglobin (HHB) family, can inhibit HCC cell proliferation [21, 28]. In this study, EdU-incorporation assay shows that ectopic CYGB can inhibit the proliferation of HCC cells with or without $pre-H_2O_2$ treatment for 12 h (**Figure 4A**). We also evaluated the proliferative index of

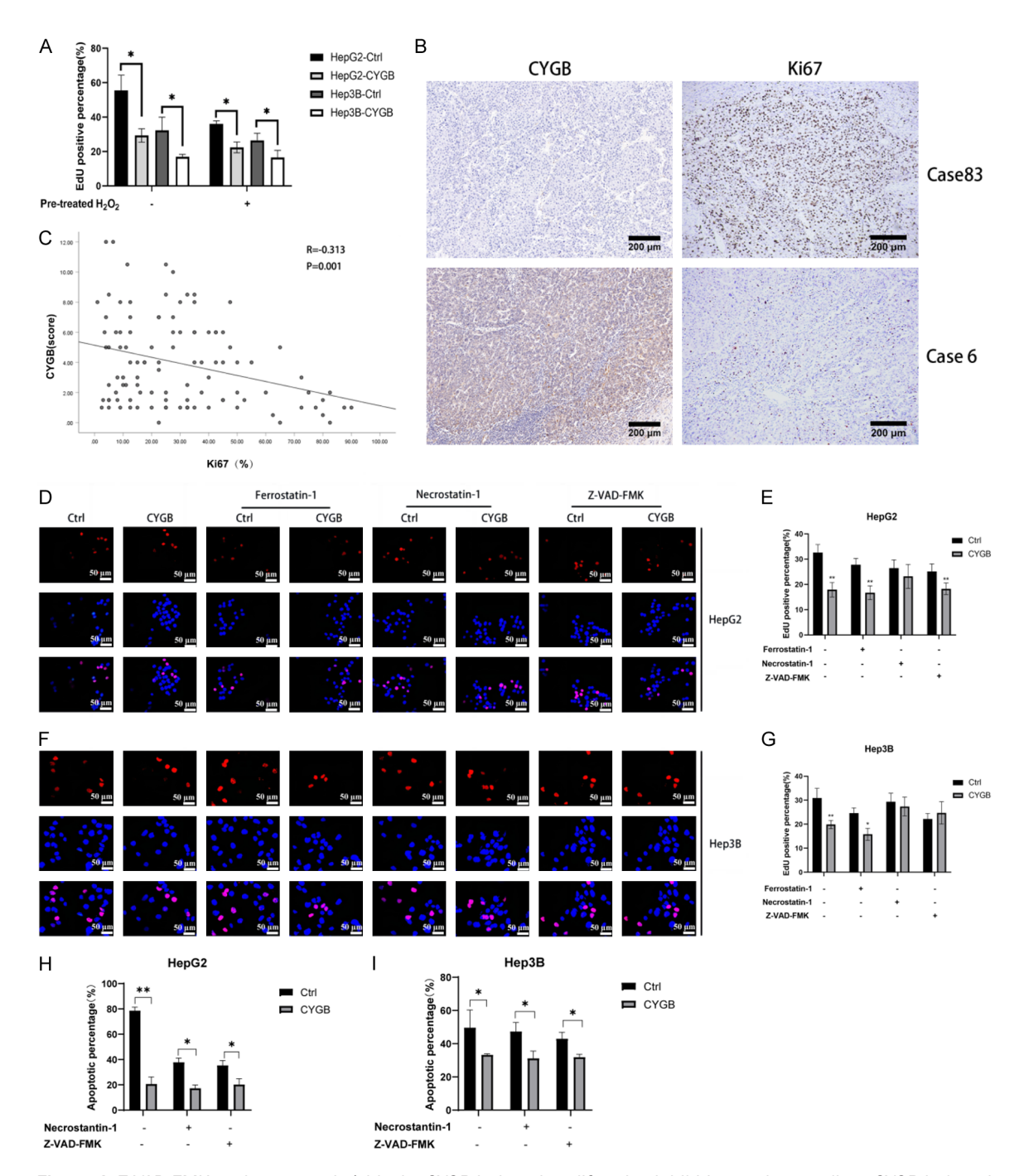


Figure 4. Z-VAD-FMK and necrostatin1 blocks CYGB-induced proliferative inhibition and neutralizes CYGB-induced apoptotic inhibition in pre- ${\rm H_2O_2}$ treated HCC cells for 12 h. (A) EdU incorporation assay evaluated the effect of CYGB upon HCC cell proliferation with or without pre- ${\rm H_2O_2}$ treatment for 12 h. The EdU positive percentage is calculated and statistically analyzed. Data are shown as Mean \pm SEM (Two-way ANOVA, "*" represents P < 0.05). (B and C) Ki-67 proliferative index and CYGB expression are assessed using IHC staining in human HCC tissues. (B) The representative images of Ki-67 and CYGB expression in the identical HCC samples are shown with 100x magnification. (C) The correlation of CYGB expression with Ki-67 proliferative index is analyzed using Pearson's correlation analysis. "r" represents the correlative coefficient. (D-G) EdU incorporation assay evaluates the effect of ferrostatin-1, necrostatin-1 and Z-VAD-FMK input upon CYGB-induced proliferative inhibition in HepG2 cells (D and E) and Hep3B cells (F and G) with pre- ${\rm H_2O_2}$ treatment for 12 h. (D and F) The representative images of EdU incorporation are shown with 400× magnification. (E and G) The EdU positive percentage are calculated and statistically analyzed. Data are shown as Mean \pm SEM (Two-way ANOVA, "*" represents P < 0.05, "**" represents P < 0.01). (H, I) Flow cytometry assesses the effect of necrostatin-1 and Z-VAD-FMK input upon CYGB-induced apoptotic inhibition in pre- ${\rm H_2O_2}$ treated HepG2 cells (H) and Hep3B (I). The apoptotic percentage are calculated and statistically analyzed. Data are shown as Mean \pm SEM (Two-way ANOVA, "*" represents P < 0.05, "**" represents P < 0.01).

Ki-67 in human HCC tissue, the results show that CYGB expression is negatively correlative with Ki-67 index (r=-0.313, P < 0.001) (Figure 4B and 4C). Ferrostatin-1, and Z-VAD-FMK (Z-VAD) are respectively the inhibitors of ferroptotic and apoptotic signaling. Necrostatin-1 (Nec-1) exhibits the dual inhibitory activity to either necroptosis or apoptosis [29]. All of these inhibitors are used to block the cell death signaling in this study, the effect of blocking cell death signaling upon CYGB-induced proliferative inhibition in pre-H₂O₂ treated HCC cells were observed (Figure 4D-G), EdUincorporation assay shows that Nec-1 interrupts CYGB-induced proliferative inhibition upon pre-H₂O₂ treated HepG2 and Hep3B cells (Figure 4D-G). Moreover, its proliferative inhibition can be blocked by Z-VAD input in pre-H₂O₂ treated Hep3B cells (Figure 4F and 4G). CYGB decreases the proliferative percentage is approximately for 7% in pre-H₂O₂ treated HepG2 cells with Z-VAD input, compared with 15% of CYGB-induced proliferative inhibition percentage in pre-H₂O₂ treated HepG2 cells without Z-VAD input (Figure 4D and 4E). The data support that Nec-1 and Z-VAD can interfere with CYGB-induced proliferative inhibition. suggesting that CYGB inhibits HCC proliferation through controlling cell death signaling. In addition, ferrostatin-1 can't be observed a significant effect upon CYGB-induced proliferative inhibition in pre-H₂O₂ treated HCC cells (Figure 4D-G). Furthermore, the effect of Nec-1 and Z-VAD upon CYGB-induced apoptotic inhibition were observed, the result showed CYGB reduces the apoptotic percentage approximately for 53% in HepG2 cells and 28% in Hep3B cells with pre-H₂O₂ treatment for 12 h (Figure 4H) and 41), whereas the percentage of CYGBinduced apoptotic inhibition is respectively 22% and 20% in pre-H₂O₂ treated HepG2 cells and Hep3B cells with Nec-1 input (Figure 4H and 41), the percentage of CYGB-induced apoptotic inhibition is respectively 18% and 9% in pre-H₂O₂ treated HepG2 cells and Hep3B cells with Z-VAD input (Figure 4H and 4I). The data indicated that Nec-1 and Z-VAD can attenuate CYGB-induced apoptotic inhibition (Figure 4H and 4I). In brief, the blockade of apoptotic signaling interferes with CYGB-induced apoptotic and proliferative inhibition in pre-H₂O₂ treated HCC cells, suggesting that CYGB functions as a maintainer of homeostasis, it overcomes oxidative damage - associated compensatory proliferation.

CYGB inactivates AKT and ERK1/2 signaling and its regulation can be interfered by necrostatin-1 or Z-VAD-FMK in pre- ${\rm H_2O_2}$ treated HCC cells

We reported that NGB inhibits HCC proliferation through controlling ERK/MAPK-activated proliferative signaling [28]. In this study, we investigate the interaction of CYGB with AKT and ERK kinase using the computing simulation modeling and molecular docking analysis. The result shows that CYGB possesses high affinity with AKT (Figure 5A) and ERK protein (Figure 5B), the docking score of CYGB is respectively -235kcal/mol with AKT and -261 kcal/mol with ERK (Figure 5A and 5B). We further observed the effect of CYGB upon AKT and ERK1/2 signaling in HCC cells without H₂O₂ treatment (Figure 5C-E). Ectopic CYGB decreases the level of phosphor-AKT by approximately 0.6, 0.7 and 0.8 folds in HepG2, Hep3B and Huh7 cells respectively, compared with the phosphor-AKT level in these control groups (Figure 5C and 5D). It also reduces phosphor-ERK1/2 level by approximately 0.6, 0.7 and 0.6 folds in HepG2, Hep3B and Huh7 cells respectively, compared with the level of phosphor-ERK1/2 in these control groups (Figure 5C and 5E). In addition, CYGB overexpression reduces p53 expression in HepG2 cells harboring with wild-type p53, as well decreases CyclinD1 expression in Huh7 cells harboring with p53 variant (Figure 5C). The regulation of CYGB upon JNK activity isn't obvious in HCC cells (Figure 5C). We further assessed that the effect of CYGB upon AKT and ERK1/2 signaling in pre-H₂O₂ treated HCC cells, the results show that ectopic CYGB inactivates AKT kinase (Figure 5F and 5G) and ERK kinase (Figure 5G and 5H), as well reduces CyclinD1 expression (Figure 5F). Furthermore, Nec-1 or Z-VAD input can disrupt CYGB-induced AKT and ERK inactivation in pre-H₂O₂ treated HCC cells (Figure 5G, 5H). In a word, we observed that Nec-1 and Z-VAD can block CYGB-induced AKT/ ERK/CyclinD1 inactivation in pre-H₂O₂ treated cells (Figure 5F-H), suggesting that CYGB targets oxidative damage-associated AKT/ERK/ CyclinD1 axis activation in a damage-associated molecule patterns (DAMPs). In addition, Nec-1 and Z-VAD also block CYGB-induced proliferative inhibition (Figure 4D-G), suggesting that CYGB inhibits cell proliferation in cell death-dependent manner. Thus we hypothesize that CYGB targets oxidative damage-associat-

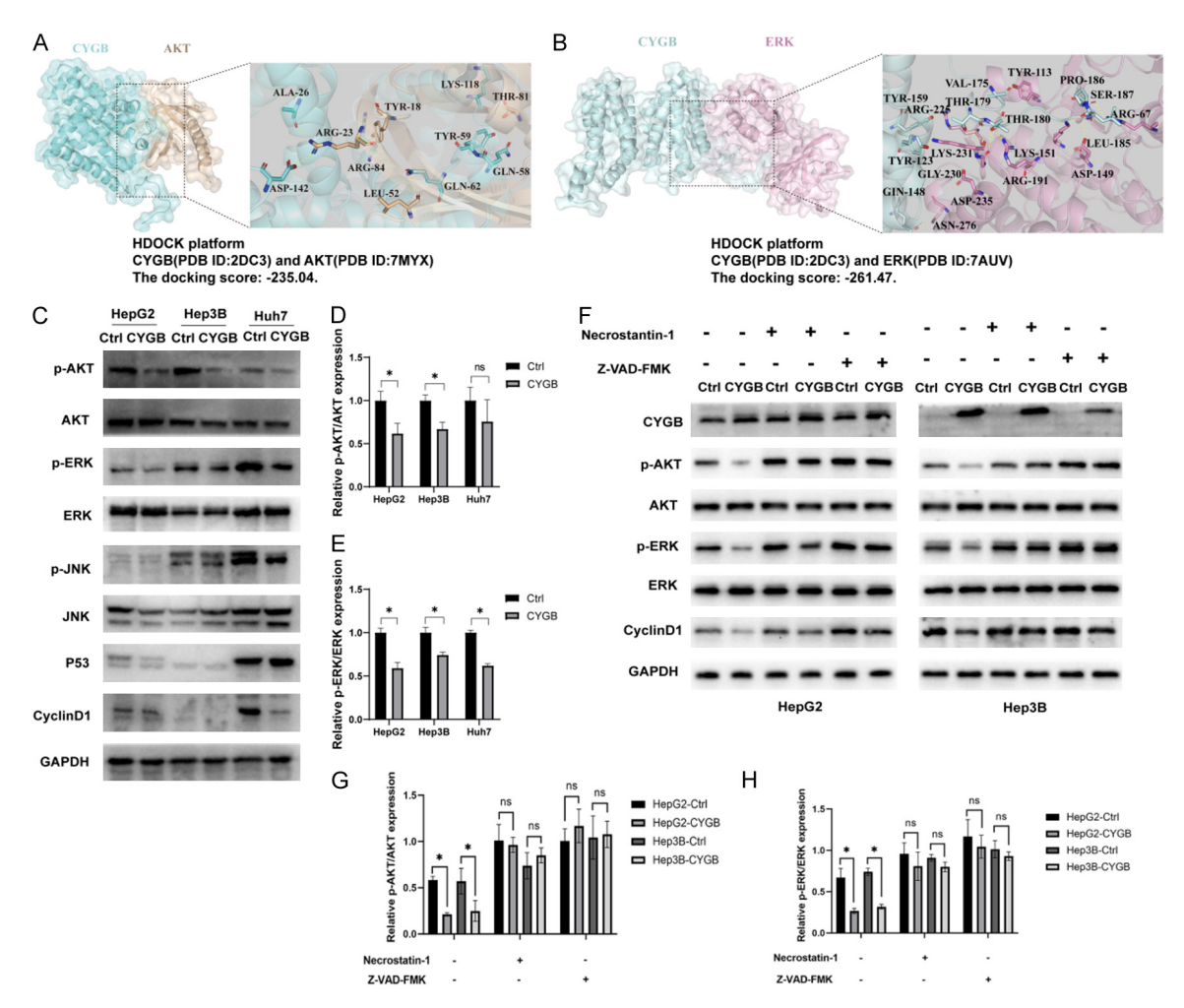


Figure 5. CYGB overexpression inactivates AKT and ERK1/2 signaling and the inhibition is disrupted by necrostatin1 and Z-VAD-FMK input in HCC cells with pre- ${\rm H_2O_2}$ treatment for 12 h. (A and B) The computing simulation docking modeling between CYGB and AKT (A) or ERK (B) is shown. The docking score reflects the affinitive capacity. "< -120 kcal/mol" implies high affinity, "> -120 kcal/mol" and "< -80 kcal/mol" implies moderate affinity, "> -50 kcal/mol" implies low affinity. The indicated protein expression is detected using immunoblotting and their average optical intensities (AOIs) of these bands are measured using ImageJ software. The expression of p-AKT or p-ERK1/2 is normalized to the total protein. The relative expression of p-AKT or p-ERK1/2 in the control group is standardized as "1". GAPDH is used as a loading control. (C-E) The effect of CYGB upon AKT and ERK1/2 signaling in HCC cells is assessed. (C and F) The representative bands are shown. (F-H) The regulation of CYGB upon AKT/ERK signaling with or without necrostatin-1 and Z-VAD-FMK was explored in pre- ${\rm H_2O_2}$ treated HCC cells. The comparatively quantification of p-AKT (D and G) or p-ERK1/2 (E and H) is shown and statistically analyzed. Data are shown as Mean \pm SEM (Two-way ANOVA, "*" represents P < 0.05).

ed AKT/ERK/CyclinD1 axis activation in a damage-associated molecule patterns (DAMPs) and inhibits HCC proliferation.

CYGB targets cell death-associated compensatory proliferation via controlling AKT/ERK/CyclinD1 axis in pre-H₂O₂ treated HCC cells

We observed that CYGB attenuates OS-induced HCC cell injury and cell proliferation and simulatanously inactivates AKT and ERK1/2 signal-

ing (Figures 2-5). Nec-1 and Z-VAD can block CYGB-induced AKT/ERK inactivation, suggesting that AKT/ERK signaling is the down-stream of cell death event (Figure 5F-H). To further investigate the correlation of CYGB-induced proliferative inhibition with CYGB-inactivated AKT/ERK axis, we strategically blocked ERK1/2 signaling using a selective inhibitor of MEK1/2 and then observed the impact of CYGB overexpression upon cell proliferation. The results show that UO126, the MEK1/2 inhibitor,

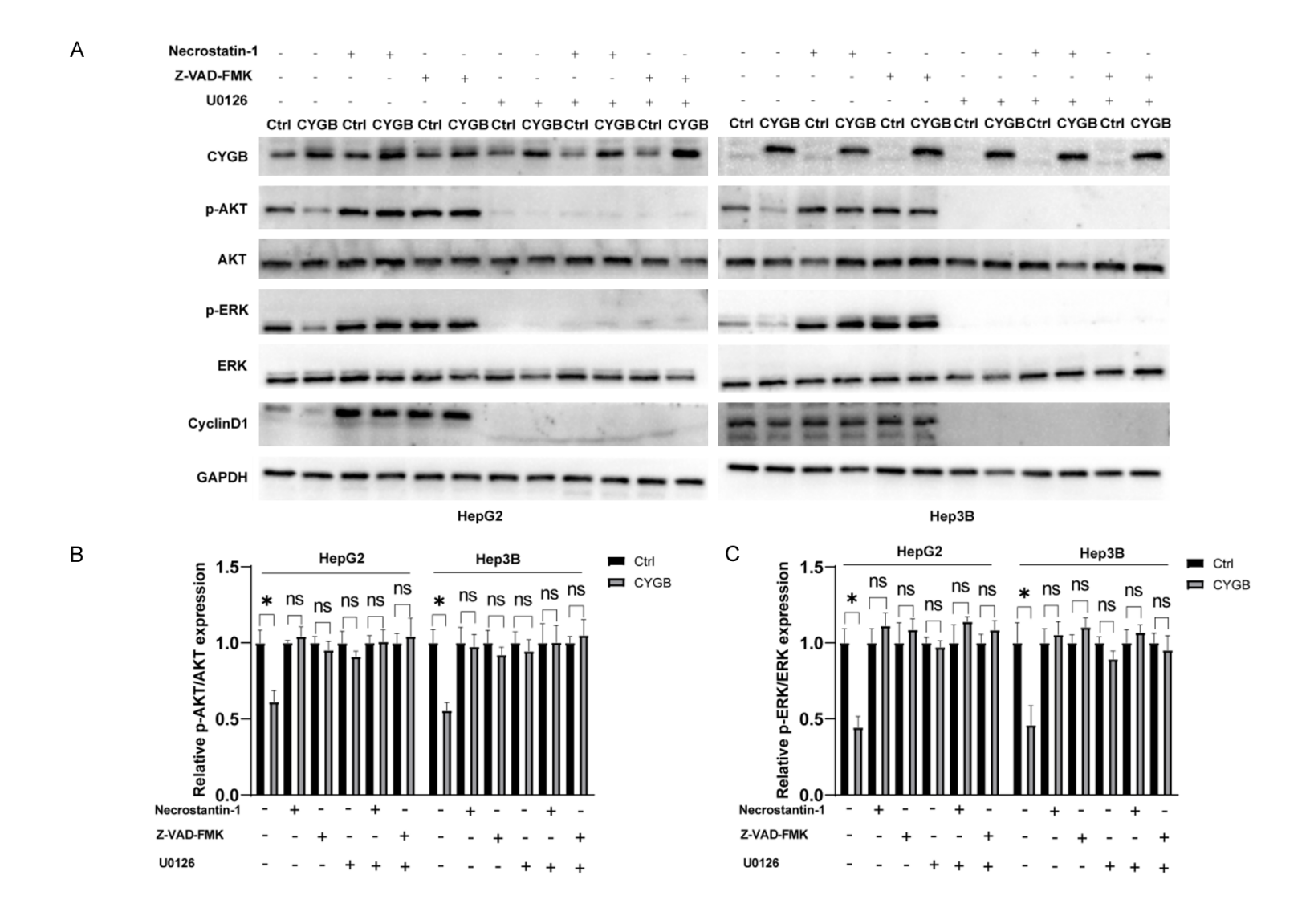
removes the inhibition of CYGB upon AKT and ERK1/2 signaling in pre-H₂O₂ treated HepG2 cells and Hep3B cells with or without Nec-1 or Z-VAD input (Figure 6A-C). CyclinD1 is a pivotal regulator of cell cycle progression and promotes the transition of G1 phase to S phase. It is specially increased by the upstream mitogenic signals including AKT or ERK1/2 kinases [30]. U0126 also disrupts the regulation of CYGB upon CyclinD1 level in pre-H₂O₂ treated HCC cells with or without Nec-1 and Z-VAD input (Figure 6A). These data suggest that CYGB controls oxidative damage and the downstream AKT/ERK/CyclinD1 axis. Furthermore, the effect of blocking ERK signaling upon CYGB-induced proliferative inhibition is observed. EdU-incorporation assay shows that U0126 also interferes CYGB-induced proliferative inhibition in pre-H₂O₂ treated HepG2 cells (Figure 6D and 6E) and Hep3B cells (Figure 6F and 6G), whether Nec-1 and Z-VAD presence or not. The data indicated that CYGB inhibits oxidative damage (Figures 2D and 2E, 3D and 3E and 4H and 4I) - associated AKT/ERK/CyclinD1 axis (Figures 5F-H and 6A-C) and HCC cell proliferation (Figures 3D and 3F, 4D-F and 6D-G). Therefore, we propose that CYGB exerts a tumor suppressor and overcomes HCC cells abnormal proliferation via targeting oxidative damage-activated AKT/ERK/CyclinD1 axis (Figure 6H).

Discussion

CYGB is deregulated in multi-malignancies by its promoter hypermethylation, its deficiency promotes inflammatory response, organ fibrosis, tumorigenesis and progression [13, 16, 20, 31]. CYGB deficiency aggravates NO accumulation and causes hepatocytes dysfunction by inhibiting cytochrome c oxidase activity in hepatocytes [32]. Cytoglobin reduction driven by TGF-β1 input leads to oxidative DNA damage and promotes non-alcoholic steatohepatitis and liver fibrosis [33]. Recombinant human cytoglobin deactivates hepatic stellate cells (HSCs) and inhibits liver fibrosis by scavenging reactive oxygen species [34]. Cygb knockout accelerates liver fibrosis and cancer development in mouse models of carcinogen-induced hepatocellular carcinoma [35]. Cytoglobin deficiency promotes the progression of hepatosteatosis to hepatocarcinogenesis through activation of the oxidative stress pathway [36]. Tp53,

a crucial regulator in immune response and cell cycle progression, is up-regulated in the cygb1 knockout liver [37]. Cygb-deficient mice exhibit the dysfunction of cancer-related genes including p53, cyclinD2 and Cdkn2a [38]. In this study, we found that CYGB is deregulated in human HCC tissues, particularly in tumor with p53 variant. Its low expression is associated with advanced clinical stage and poor differentiation, as well predicts a worse prognosis (Figure 1; Table 1). Its expression is negatively correlative with Ki-67 proliferative index (Figure 4B and 4C), the low expression of CYGB is associated with a large tumor mass (Table 1), suggesting that CYGB exhibits anti-tumor effect and inhibit tumor growth. Therefore, these findings support that CYGB functions as a tumor suppressor in HCC genesis and progression. Although the regulation of CYGB upon p53 and AKT/ERK axis isn't consistent, the interaction of CYGB with p53 should be further explored in the signaling network of HCC development. The previous studies indicated that the combining evaluation of CYGB and SOX7 can be capable of predicting the prognostic outcomes of bladder cancer patients [18]. Cygb loss may contribute to tumor recurrence and a worse prognosis in gliomas. It may serve as an independent predictive factor in the prognosis of glioma patients [39]. These data support that the supervision of CYGB expression can be a prognostic indicator in predicting tumor outcomes. In addition, CYGB can be up-regulated and be responsive to various stresses [13, 14]. We found that the expression of CYGB is consistent with serum AST/ALT level in human HCC patients in this study (Table 1), we presume that CYGB is also a stress-responsive protein and reflects the liver function of these HCC patients to a certain content.

Although the previous studies have demonstrated the anti-neoplastic effect of CYGB in tumorigenesis and development, the underlying mechanisms is elusive. CYGB deficiency sensitizes melanoma cells to a GPX4 inhibitor of (1S, 3R)-RAS-selective lethal small molecule (RSL3) -mediated ferroptosis, as well activates NOD-, LRR- and pyrin domain-containing protein 3 (NLRP3) inflammasome and induces the pyroptosis of melanoma cells [20]. CYGB expression enhances heme-oxygenase 1 (HO-1) and NRF2 protein expression levels and protects melanoma cells from RONS-induced



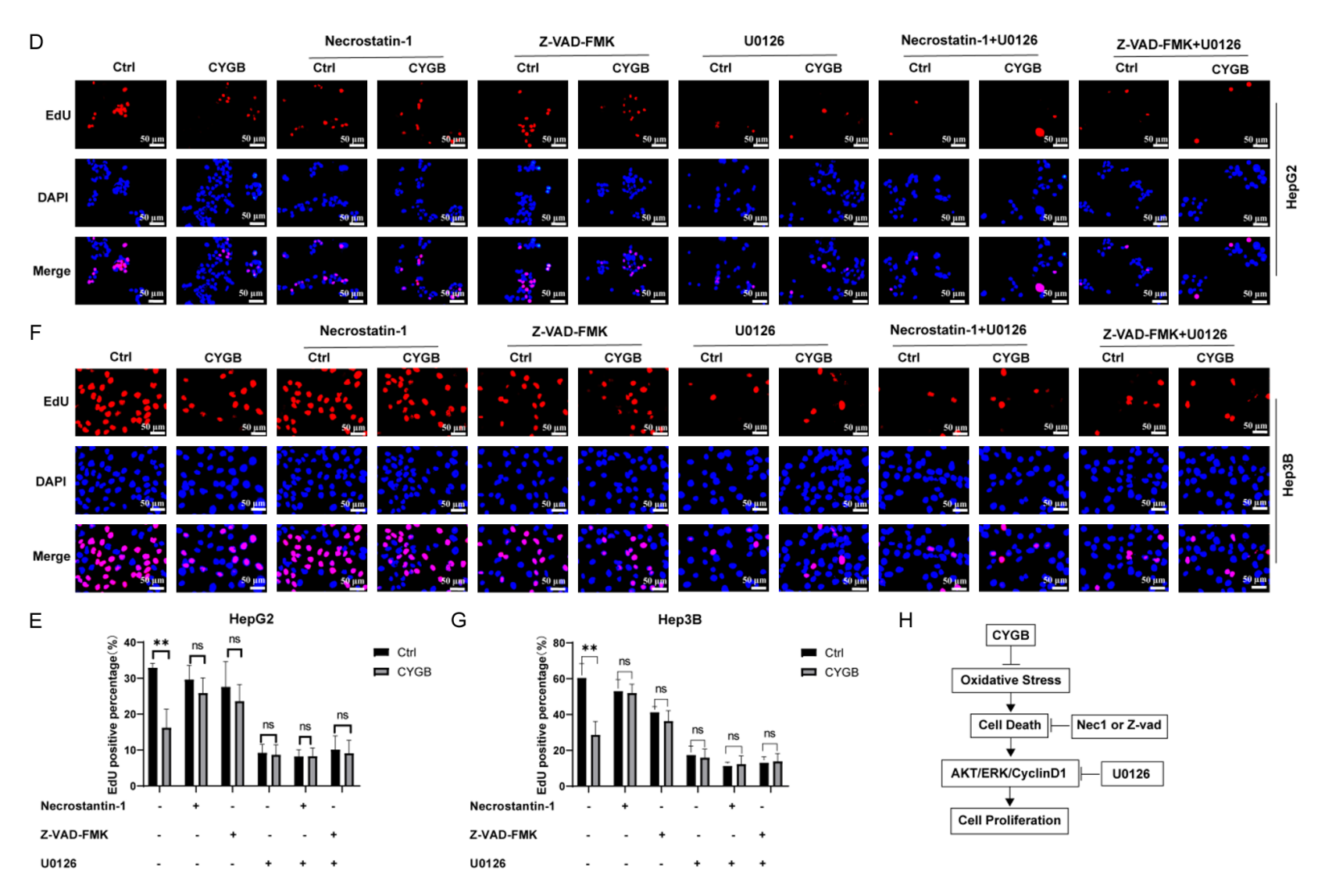


Figure 6. CYGB controls oxidative damage-associated AKT/ERK1/2 activation and inhibits cell proliferation in HCC cells. (A-C) The interaction of CYGB-inactivated AKT/ERK signaling with pre- H_2O_2 -induced cell death is investigated. These indicated protein level was assessed using immunoblotting. The relative expression of p-AKT or p-ERK1/2 is normalized to the total protein. The relative expression of p-AKT or p-ERK1/2 in the control group is standardized as "1". GAPDH is used as a loading control. (A) The representative bands are shown. (B and C) The comparatively quantification of p-AKT (B) or p-ERK1/2 (C) is shown and statistically analyzed. Data are shown as Mean \pm SEM (Two-way ANOVA, "*" represents P < 0.05). (D-G) The regulation of CYGB-inactivated AKT/ERK signaling upon CYGB-induced proliferative inhibition is tested. (D and F) The representative fluorescent images of EdU-incorporation assay are shown with 400x magnification. (E and G) EdU

positive percentage is calculated and statistically analyzed. Data are shown as Mean \pm SEM (Two-way ANOVA, "**" represents P < 0.01). (H) The mechanistic graphic is depicted and shown.

apoptosis [19]. CYGB-p53 and GPD1L-HIF1a axis deregulation induced by ectopic miR-210-3p protects triple-negative breast cancer from serum starvation-induced cell apoptosis [17]. In this study, we found that CYGB overexpression decreases these intracellular enzymes release from pre-H2O2 treated HCC cells (Figure 2D and 2E) and protects HCC cells from pre-H₂O₂-induced apoptosis and DNA damage (Figure 3B-E). Our findings propose that CYGB functions as an anti-oxidant enzyme and prevents OS-induced cell death. The previous studies reported that ectopic CYGB expression suppresses proliferation in breast cancer cell lines and inhibits xenograft tumor growth in vivo [16]. CYGB deficiency prevents the myotubes formation in myogenic progenitor cells and muscle regeneration [40]. Cygb overexpression or recombinant human CYGB (rhCYGB) induces G1 phase arrest in pancreatic cancer cells, as well blocks cell proliferation and ROS production provoked by H2O2 challenge [15]. Cygb expression induced by DNA damage can stabilize p53 and mediate G1 arrest [41]. In this study, we found that CYGB overexpression reduces HCC cell viability in time-dependent pattern (Figure 2C) and decrease HCC cell proliferation with or without pre-H₂O₂ treatment in vitro (Figure 4A). CYGB expression is negatively associated with Ki-67 proliferative index in human HCC tissues (Figure 4B, 4C). CYGB overexpression can inhibit DNA damage and simultaneously induce G1 phase arrest in pre-H₂O₂ treated HCC cells (Figure 3D-F). Furthermore, we found that necrostatin-1 and Z-VAD-FMK, the inhibitors of cell death signaling, can mitigate CYGB-induced apoptotic inhibition in pre-H₂O₂ treated HCC cells (Figure 4H and 4I). Moreover, necrostatin-1 or Z-VAD-FMK input alleviates CYGB proliferative inhibition upon pre-H₂O₂ treated HCC cells (Figure 4D-G). These data suggest that CYGB inhibits OS-induced cell injury and compensatory proliferation, as a result, it exerts an anti-tumor effect via maintaining hemeostasis against HCC progression.

Ectopic CYGB expression deregulates multiple cancer-associated genes, including the mTORC1 and AKT/mTOR signaling pathways, its regulative roles involve in epithelial-mesenchy-

mal transition (EMT), inflammatory response and DNA damage repair in melanoma cells [42]. CYGB overexpression deregulates PI3K/ AKT/mTOR signaling and inhibits cell proliferation and migration in fibroblast cells [43]. Cygb deficiency elevates extracellular signal-regulated kinase and Akt activity and promotes cancer cell proliferation, its deficiency increases liver and lung cancer incidence in mice exposed to DEN [38], Intranasal administration of cytoglobin can modulate p38 MAPK signaling-mediated apoptosis and improves hypoxic-ischemia brain damage in neonatal rats [44]. In this study, we found that CYGB significantly deregulates AKT and ERK signaling in HCC cells with or without pre- H_2O_2 treatment (Figure 5). AKT and ERK are the pivotal tumor driver genes and are co-activated in multi-malignancies. Concanavalin A activates Akt/ERK/CyclinD1 axis and promotes angiogenesis and proliferation in endothelial cells [45]. High lipocalin 2 expression activates SRC/AKT/ERK-mediated antiapoptotic program and induces colorectal cancer (CRC) resistance to 5-fluorouracil therapy [46]. Damage-associated molecular patterns (DAMPs) provide a protective mechanism in tumor relapse, metastasis and resistance to chemotherapy, cisplatin- and oxaliplatininduced damage activates AKT/ERK/Cyclin-D1 axis and promotes cholangiocarcinoma progression [47]. Emerging studies further indicate that the dual inhibition of PI3K/AKT/mTOR and RAF/MEK/ERK signaling provide a novel therapeutic regimen in multi-drug resistance cancers. The pharmaceutical dual blockade of EGFR/ERK and PI3K/AKT signaling shows a synergistically therapeutic effect against glioblastoma [50]. Costunolide, a dual inhibitor of MEK1 and AKT1/2, overcomes MEK1 and AKT1/2 abnormal activation-induced by EGFR-TKI therapy and re-sensitizes lung cancer to osimertinib therapy [51]. Agrimoniin has a dual inhibitive activity of AKT and ERK kinases and exhibits an anti-pancreatic cancer effect by inducing apoptosis and cell cycle arrest [52]. Alpelisib is a selective PIK3CA inhibitor, it reduces the growth of HCC with PIK3CA mutation in mouse model by inhibiting MAPK and AKT cascades [53]. In this study, we found that CYGB simultaneously inactivates AKT and ERK

kinase in HCC cells (**Figure 5**) and its inhibition can be blocked by necrostatin-1 and Z-VAD-FMK input in pre-H₂O₂ treated HCC cells (**Figure 5**). Furthermore, our data shows the blockade of ERK1/2 signaling disrupts CYGB-induced proliferative inhibition upon pre-H₂O₂ treated HCC cells, whether the interruption of cell death signaling or not (**Figure 6**). Therefore, our findings elucidate that CYGB inhibits OS-induced cell damage and subsequently compensatory proliferation via inactivating AKT/ERK/cyclinD1 axis in HCC cells.

This study demonstrated that the role and underlying mechanisms of cytoglobin against HCC development. CYGB deficiency is associated with undesirable bio-behaviors and predicts a worse prognosis. The mechanistic investigation reveals that CYGB overcomes oxidative damage-activated AKT/ERK/CyclinD1 axis and compensatory proliferation. The observed effects and mechanistic insights support that CYGB restoration may provide a promising therapeutic rationale against advanced HCC. In particular, the combination strategy including CYGB which targets AKT/ERK aberrant activation to overcome HCC resistance to conventional chemotherapies merits to be further explored.

Acknowledgements

This project was granted by the National Natural Science Foundation of China (82060565, 81860544) and the PhD Research Start-up Foundation of Affiliated Hospital of Guizhou Medical University (gyflbsky-2024-13).

Disclosure of conflict of interest

None.

Address correspondence to: Dr. Jun Zhang, Department of Pathology, The Affiliated Hospital of Guizhou Medical University, No. 28 Gui Yi Street, Guiyang 550004, Guizhou, China. E-mail: zhangjun8989@gmc.edu.cn

References

- [1] Allameh A, Niayesh-Mehr R, Aliarab A, Sebastiani G and Pantopoulos K. Oxidative stress in liver pathophysiology and disease. Antioxidants (Basel) 2023; 12: 1653.
- [2] Liu Y, Zhang J, Liu H, Guan G, Zhang T, Wang L, Qi X, Zheng H, Chen CC, Liu J, Cao D, Lu F and

- Chen X. Compensatory upregulation of aldoketo reductase 1b10 to protect hepatocytes against oxidative stress during hepatocarcinogenesis. Am J Cancer Res 2019; 9: 2730-2748.
- [3] Bartolini D, Dallaglio K, Torquato P, Piroddi M and Galli F. Nrf2-P62 Autophagy pathway and its response to oxidative stress in hepatocellular carcinoma. Transl Res 2018; 193: 54-71.
- [4] Chen XF, Tian MX, Sun RQ, Zhang ML, Zhou LS, Jin L, Chen LL, Zhou WJ, Duan KL, Chen YJ, Gao C, Cheng ZL, Wang F, Zhang JY, Sun YP, Yu HX, Zhao YZ, Yang Y, Liu WR, Shi YH, Xiong Y, Guan KL and Ye D. Sirt5 inhibits peroxisomal Acox1 to prevent oxidative damage and is downregulated in liver cancer. EMBO Rep 2018; 19: e45124.
- [5] Chibaya L, Karim B, Zhang H and Jones SN. Mdm2 phosphorylation by Akt regulates the P53 response to oxidative stress to promote cell proliferation and tumorigenesis. Proc Natl Acad Sci U S A 2021; 118: e2003193118.
- [6] Huang Z, Zhou L, Duan J, Qin S, Jiang J, Chen H, Wang K, Liu R, Yuan M, Tang X, Nice EC, Wei Y, Zhang W and Huang C. Oxidative stress promotes liver cancer metastasis via Rnf25mediated E-Cadherin protein degradation. Adv Sci (Weinh) 2024; 11: e2306929.
- [7] Wang J, McGrail DJ, Bhupal PK, Zhang W, Lin KY, Ku YH, Lin T, Wu H, Tsai KC, Li K, Peng CY, Finegold MJ, Lin SY and Tsai RYL. Nucleostemin modulates outcomes of hepatocellular carcinoma via a tumor adaptive mechanism to genomic stress. Mol Cancer Res 2020; 18: 723-734.
- [8] Banerjee P, Gaddam N, Chandler V and Chakraborty S. Oxidative stress-induced liver damage and remodeling of the liver vasculature. Am J Pathol 2023; 193: 1400-1414.
- [9] Esparza-Baquer A, Labiano I, Sharif O, Agirre-Lizaso A, Oakley F, Rodrigues PM, Zhuravleva E, O'Rourke CJ, Hijona E, Jimenez-Agüero R, Riaño I, Landa A, La Casta A, Zaki MYW, Munoz-Garrido P, Azkargorta M, Elortza F, Vogel A, Schabbauer G, Aspichueta P, Andersen JB, Knapp S, Mann DA, Bujanda L, Banales JM and Perugorria MJ. Trem-2 defends the liver against hepatocellular carcinoma through multifactorial protective mechanisms. Gut 2021; 70: 1345-1361.
- [10] Hamza AA, Heeba GH, Hamza S, Abdalla A and Amin A. Standardized extract of ginger ameliorates liver cancer by reducing proliferation and inducing apoptosis through inhibition oxidative stress/inflammation pathway. Biomed Pharmacother 2021; 134: 111102.
- [11] Mathai C, Jourd'heuil FL, Lopez-Soler RI and Jourd'heuil D. Emerging perspectives on cytoglobin, beyond no dioxygenase and peroxidase. Redox Biol 2020; 32: 101468.

- [12] Zweier JL, Hemann C, Kundu T, Ewees MG, Khaleel SA, Samouilov A, Ilangovan G and El-Mahdy MA. Cytoglobin has potent superoxide dismutase function. Proc Natl Acad Sci U S A 2021: 118: e2105053118.
- [13] De Backer J, Razzokov J, Hammerschmid D, Mensch C, Hafideddine Z, Kumar N, van Raemdonck G, Yusupov M, Van Doorslaer S, Johannessen C, Sobott F, Bogaerts A and Dewilde S. The effect of reactive oxygen and nitrogen species on the structure of cytoglobin: a potential tumor suppressor. Redox Biol 2018; 19: 1-10.
- [14] De Backer J, Maric D, Bosman M, Dewilde S and Hoogewijs D. A reliable set of reference genes to normalize oxygen-dependent cytoglobin gene expression levels in melanoma. Sci Rep 2021; 11: 10879.
- [15] Hoang DV, Thuy LTT, Hai H, Hieu VN, Kimura K, Oikawa D, Ikura Y, Dat NQ, Hoang TH, Sato-Matsubara M, Dong MP, Hanh NV, Uchida-Kobayashi S, Tokunaga F, Kubo S, Ohtani N, Yoshizato K and Kawada N. Cytoglobin attenuates pancreatic cancer growth via scavenging reactive oxygen species. Oncogenesis 2022; 11: 23.
- [16] Feng Y, Wu M, Li S, He X, Tang J, Peng W, Zeng B, Deng C, Ren G and Xiang T. The epigenetically downregulated factor Cygb suppresses breast cancer through inhibition of glucose metabolism. J Exp Clin Cancer Res 2018; 37: 313.
- [17] Du Y, Wei N, Ma R, Jiang S and Song D. A Mir-210-3p regulon that controls the warburg effect by modulating Hif-1 α and P53 activity in triple-negative breast cancer. Cell Death Dis 2020; 11: 731.
- [18] Zhang J, Zhang W, Liu J, Liu Y, Jiang Y, Ainiwaer A, Chen H, Gu Z, Chen H, Mao S, Guo Y, Xu T, Xu Y, Wu Y, Yao X and Yan Y. Sox7 inhibits the malignant progression of bladder cancer via the Dnmt3b/Cygb axis. Mol Biomed 2024; 5: 36.
- [19] De Backer J, Lin A, Berghe WV, Bogaerts A and Hoogewijs D. Cytoglobin inhibits non-thermal plasma-induced apoptosis in melanoma cells through regulation of the Nrf2-mediated antioxidant response. Redox Biol 2022; 55: 102399.
- [20] De Backer J, Maric D, Zuhra K, Bogaerts A, Szabo C, Vanden Berghe W and Hoogewijs D. Cytoglobin silencing promotes melanoma malignancy but sensitizes for ferroptosis and pyroptosis therapy response. Antioxidants (Basel) 2022; 11: 1548.
- [21] Zhang J, Pei Y, Yang W, Yang W, Chen B, Zhao X and Long S. Cytoglobin ameliorates the stemness of hepatocellular carcinoma via coupling oxidative-nitrosative stress signals. Mol Carcinog 2019; 58: 334-343.

- [22] Ahodantin J, Bou-Nader M, Cordier C, Megret J, Soussan P, Desdouets C and Kremsdorf D. Hepatitis B virus X protein promotes DNA damage propagation through disruption of liver polyploidization and enhances hepatocellular carcinoma initiation. Oncogene 2019; 38: 2645-2657.
- [23] Sung YN, Kim D and Kim J. P53 immunostaining pattern is a useful surrogate marker for Tp53 gene mutations. Diagn Pathol 2022; 17: 92.
- [24] Yuan X, Yang L, Gao T, Gao J, Wang B, Liu C and Yuan W. Yinchen Wuling powder attenuates non-alcoholic steatohepatitis through the inhibition of the Shp2/Pi3k/Nlrp3 pathway. Front Pharmacol 2024; 15: 1423903.
- [25] Tang Z, Li C, Kang B, Gao G, Li C and Zhang Z. Gepia: a web server for cancer and normal gene expression profiling and interactive analyses. Nucleic Acids Res 2017; 45: W98-W102.
- [26] Yan Y, Tao H, He J and Huang SY. The hdock server for integrated protein-protein docking. Nat Protoc 2020; 15: 1829-1852.
- [27] He L, Zhu C, Jia J, Hao XY, Yu XY, Liu XY and Shu MG. Adsc-Exos containing Malat1 promotes wound healing by targeting Mir-124 through activating Wnt/B-Catenin pathway. Biosci Rep 2020; 40: BSR20192549.
- [28] Zhang J, Lan SJ, Liu QR, Liu JM and Chen XQ. Neuroglobin, a novel intracellular hexa-coordinated globin, functions as a tumor suppressor in hepatocellular carcinoma via Raf/Mapk/ Erk. Mol Pharmacol 2013; 83: 1109-19.
- [29] Dong L, Liang F, Lou Z, Li Y, Li J, Chen Y, Ding J, Jiang B, Wu C, Yu H, Liu Y, Zhang W, Lu Y and Wu M. Necrostatin-1 alleviates lung ischemiareperfusion injury via inhibiting necroptosis and apoptosis of lung epithelial cells. Cells 2022; 11: 3139.
- [30] Wang C, Huang X, Sun K, Li X, Feng D, Nakamura Y and Qi H. Whey protein and flaxseed gum co-encapsulated fucoxanthin promoted tumor cells apoptosis based on mapk-Pi3k/Akt regulation on Huh-7 cell xenografted nude mice. Int J Biol Macromol 2024; 278: 134838.
- [31] Porto E, Loula P, Strand S and Hankeln T. Molecular analysis of the human cytoglobin mrna isoforms. J Inorg Biochem 2024; 251: 112422.
- [32] Okina Y, Sato-Matsubara M, Kido Y, Urushima H, Daikoku A, Kadono C, Nakagama Y, Nitahara Y, Hoang TH, Thuy LTT, Matsubara T, Ohtani N, Ikeda K, Yoshizato K and Kawada N. Nitric oxide derived from cytoglobin-deficient hepatic stellate cells causes suppression of cytochrome C oxidase activity in hepatocytes. Antioxid Redox Signal 2023; 38: 463-479.
- [33] Okina Y, Sato-Matsubara M, Matsubara T, Daikoku A, Longato L, Rombouts K, Thanh

- Thuy LT, Ichikawa H, Minamiyama Y, Kadota M, Fujii H, Enomoto M, Ikeda K, Yoshizato K, Pinzani M and Kawada N. Tgf-B1-driven reduction of Cytoglobin leads to oxidative DNA damage in stellate cells during non-alcoholic steatohepatitis. J Hepatol 2020; 73: 882-895.
- [34] Dat NQ, Thuy LTT, Hieu VN, Hai H, Hoang DV, Thi Thanh Hai N, Thuy TTV, Komiya T, Rombouts K, Dong MP, Hanh NV, Hoang TH, Sato-Matsubara M, Daikoku A, Kadono C, Oikawa D, Yoshizato K, Tokunaga F, Pinzani M and Kawada N. Hexa histidine-tagged recombinant human cytoglobin deactivates hepatic stellate cells and inhibits liver fibrosis by scavenging reactive oxygen species. Hepatology 2021; 73: 2527-2545.
- [35] Thuy LTT, Hai H and Kawada N. Role of cytoglobin, a novel radical scavenger, in stellate cell activation and hepatic fibrosis. Clin Mol Hepatol 2020; 26: 280-293.
- [36] Thuy le TT, Matsumoto Y, Thuy TT, Hai H, Suoh M, Urahara Y, Motoyama H, Fujii H, Tamori A, Kubo S, Takemura S, Morita T, Yoshizato K and Kawada N. Cytoglobin deficiency promotes liver cancer development from hepatosteatosis through activation of the oxidative stress pathway. Am J Pathol 2015; 185: 1045-60.
- [37] Schlosser A, Helfenrath K, Wisniewsky M, Hinrichs K, Burmester T and Fabrizius A. The Knockout of cytoglobin 1 in zebrafish (Danio Rerio) alters lipid metabolism, iron homeostasis and oxidative stress response. Biochim Biophys Acta Mol Cell Res 2023; 1870: 119558.
- [38] Thuy le TT, Morita T, Yoshida K, Wakasa K, lizuka M, Ogawa T, Mori M, Sekiya Y, Momen S, Motoyama H, Ikeda K, Yoshizato K and Kawada N. Promotion of liver and lung tumorigenesis in den-treated cytoglobin-deficient mice. Am J Pathol 2011; 179: 1050-60.
- [39] Xu HW, Huang YJ, Xie ZY, Lin L, Guo YC, Zhuang ZR, Lin XP, Zhou W, Li M, Huang HH, Wei XL, Man K and Zhang GJ. The expression of cytoglobin as a prognostic factor in gliomas: a retrospective analysis of 88 patients. BMC Cancer 2013; 13: 247.
- [40] Singh S, Canseco DC, Manda SM, Shelton JM, Chirumamilla RR, Goetsch SC, Ye Q, Gerard RD, Schneider JW, Richardson JA, Rothermel BA and Mammen PP. Cytoglobin modulates myogenic progenitor cell viability and muscle regeneration. Proc Natl Acad Sci U S A 2014; 111: E129-38.
- [41] John R, Chand V, Chakraborty S, Jaiswal N and Nag A. DNA damage induced activation of Cygb stabilizes P53 and mediates G1 arrest. DNA Repair (Amst) 2014; 24: 107-112.

- [42] De Backer J and Hoogewijs D. The cytoglobindependent transcriptome in melanoma indicates a protective function associated with oxidative stress, inflammation and cancer-associated pathways. Sci Rep 2024; 14: 18175.
- [43] Demirci S, Doğan A, Apdik H, Tuysuz EC, Gulluoglu S, Bayrak OF and Şahin F. Cytoglobin inhibits migration through Pi3k/Akt/Mtor pathway in fibroblast cells. Mol Cell Biochem 2018; 437: 133-142.
- [44] Yang H, Tian S, Xie L, Chen Y and Ma L. Intranasal administration of cytoglobin modifies human umbilical cord-derived mesenchymal stem cells and improves hypoxic-ischemia brain damage in neonatal rats by modulating p38 mapk signaling-mediated apoptosis. Mol Med Rep 2020; 22: 3493-3503.
- [45] Li JZ, Zhou XX, Wu WY, Qiang HF, Xiao GS, Wang Y and Li G. Concanavalin a promotes angiogenesis and proliferation in endothelial cells through the Akt/Erk/Cyclin D1 axis. Pharm Biol 2022; 60: 65-74.
- [46] Zhang W, Pan R, Lu M, Zhang Q, Lin Z, Qin Y, Wang Z, Gong S, Lin H, Chong S, Lu L, Liao W and Lu X. Epigenetic induction of lipocalin 2 expression drives acquired resistance to 5-fluorouracil in colorectal cancer through integrin B3/Src pathway. Oncogene 2021; 40: 6369-6380.
- [47] Songjang W, Nensat C, Nernpermpisooth N, Seenak P, Pankhong P, Jumroon N, Kumphune S and Jiraviriyakul A. Tumor-promoting activity and proteomic profiling of cisplatin/oxaliplatinderived damps in cholangiocarcinoma cells. Int J Mol Sci 2022; 23: 10540.
- [48] Chen MY, Hsu CH, Setiawan SA, Tzeng DTW, Ma HP, Ong JR, Chu YC, Hsieh MS, Wu ATH, Tzeng YM and Yeh CT. Ovatodiolide and antrocin synergistically inhibit the stemness and metastatic potential of hepatocellular carcinoma via impairing ribosome biogenesis and modulating Erk/Akt-Mtor signaling axis. Phytomedicine 2023; 108: 154478.
- [49] Rosenberg L, Yoon CH, Sharma G, Bertagnolli MM and Cho NL. Sorafenib inhibits proliferation and invasion in desmoid-derived cells by targeting Ras/Mek/Erk and Pi3k/Akt/Mtor pathways. Carcinogenesis 2018; 39: 681-688.
- [50] Guo T, Wu C, Zhang J, Yu J, Li G, Jiang H, Zhang X, Yu R and Liu X. Dual blockade of Egfr and Pi3k signaling pathways offers a therapeutic strategy for glioblastoma. Cell Commun Signal 2023; 21: 363.
- [51] Tian X, Wang R, Gu T, Ma F, Laster KV, Li X, Liu K, Lee MH and Dong Z. Costunolide is a dual inhibitor of Mek1 and Akt1/2 that overcomes osimertinib resistance in lung cancer. Mol Cancer 2022; 21: 193.

CYGB targets HCC proliferation in a damage-dependent manner

- [52] Zhang X, Chen J, Xi B, Liu Y, Wang S, Gu L, Zhao H, Tao L, Hua Y, Wang Y and Chen M. Agrimoniin is a dual inhibitor of Akt and Erk pathways that inhibit pancreatic cancer cell proliferation. Phytother Res 2023; 37: 4076-4091.
- [53] Xu H, Chen K, Shang R, Chen X, Zhang Y, Song X, Evert M, Zhong S, Li B, Calvisi DF and Chen X. Alpelisib combination treatment as novel targeted therapy against hepatocellular carcinoma. Cell Death Dis 2021; 12: 920.